3D PARTICLE VOLUME TOMOGRAPHIC RECONSTRUCTION BASED ON MARKED POINT PROCESS: APPLICATION TO TOMO-PIV IN FLUID MECHANICS

R. Ben Salah[1,2], *O. Alata*[3], *L. Thomas*[1], *B. Tremblais*[2], *L. David*[1]

[1]University of Poitiers, Pprime Institute, Fluid, Thermic and Combustion Department, CNRS 3346
[2]University of Poitiers, Xlim Laboratory, SIC Department, CNRS 7252
[3]University Jean Monnet of Saint-Etienne, Hubert Curien Laboratory, CNRS 5516

riadh.ben.salah@univ-poitiers.fr

ABSTRACT

In recent years, marked point processes have received a great deal of attention. They were applied with success to extract objects in large data sets as those obtained in remote sensing frameworks or biological studies. We propose in this paper a method based on marked point processes to reconstruct volumes of 3D particles from images of 2D particles provided by the Tomographic Particle Image Velocimetry (Tomo-PIV) technique. Unlike other reconstruction methods, our approach allows us to solve the problem in a parsimonious way. It facilitates the introduction of prior knowledge and naturally solves the memory problem which is inherent to pixel based approach used by classical tomographic reconstruction methods. The best reconstruction is found by minimizing an energy function which defines the marked point process. In order to avoid local minima, we use a simulated annealing algorithm. Results are presented on simulated data.

Index Terms— Marked Point Processes, Tomography Reconstruction, Simulated Annealing, Tomo-PIV, Fluid Mechanics.

1. INTRODUCTION

The growth in size and complexity of experimental data provided by the Tomo-PIV technique in fluid mechanics research, and the need of better data reconstruction requires the development of new approaches to warrant optimal scientific exploitation of the instruments. This paper focuses on the reconstruction of volumes of 3D particles, formulated in a marked point process reconstruction framework.

The Tomo-PIV technique was proposed by Elsinga et al [1]. Based on PIV and a multi-sensor recording, this approach allows instantaneous measurement of the three velocity components in a volume. The size of the measurement volume is completely flexible and can be adapted to measure small volumes of a few mm^3 as well as large volumes. However, the depth of focus remains a limiting factor. The principle of the Tomo-PIV is based on the computation of the velocity vector field of a flow from the displacement of the tracer particles recorded on several images. It consists on adding tracer particles in the stream of interest and to illuminate a portion of the flow volume by a laser source. The light scattered by the particles is captured by several high-resolution digital cameras (approximately 3 to 6, usually 4) from different viewing angles. The information on the line of sight of each pixel in a camera, through the examined volume, is described by an approximation (polynomial) made from 3D calibration procedure. Thus, the projection set of each camera is supplied to a 3D reconstruction algorithm (Fig.1). Finally, the

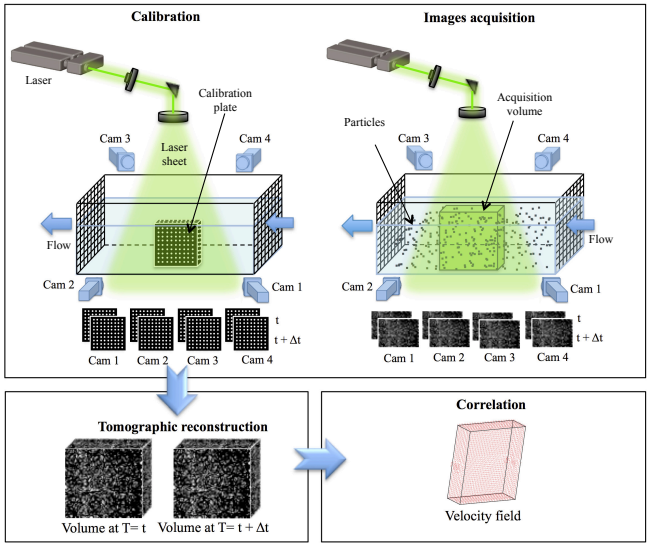

Fig. 1. Tomo-PIV principle.

sequences of 3D particle volumes are used to estimate the sequences of velocity fields using advanced cross-correlations techniques.

Due to the very small number of views, the 3D reconstruction step is an inverse ill-posed problem. Most solutions rely on the use of tomographic algebraic reconstruction methods (ART for Algebraic Reconstruction Technique, MART for Multiplicative ART, SMART for Simultaneous MART, ...) [2, 3, 4, 5]. Another solution based on a hybrid algorithm was proposed recently. The algorithm is similar to MART but it iteratively reconstructs 3D particle locations by comparing the recorded images with the projections calculated from the particle distribution in the volume [6]. Nevertheless, already proposed Tomographic reconstruction techniques don't sufficiently take into account the particular shape of objects to be reconstructed. In addition to the high density of particles in images, noise is an unfavorable element to a high reconstruction quality. Given the size of data, the processing time of the methods and the memory usage are very high. To solve these problems, a solution based on the parsimony of the volume of particles can be considered. Thus, a method

The current work has been conducted as part of the AFDAR project, Advanced Flow Diagnostics for Aeronautical research, funded by the European Commission program FP7, grant n°265695 and the FEDER project n°34754

to reconstruct volumes of 3D particles based on "object" processes, as marked point processes, seems particularly well suited.

This paper is organized as follows: in section 2, after some recalls on marked point processes, we provide the new model that can be used for the reconstruction of 3D particles. Experimental results are given in section 3. In section 4, we conclude the paper and give some prospects for the work.

2. A MARKED POINT PROCESS FOR 3D PARTICLE VOLUME RECONSTRUCTION

2.1. Basics of marked point processes

In this section, we recall the basic ideas of point processes (PP) and marked point processes (MPP). For further details we recommend [7, 8, 9, 10].

Let $K \subset \mathbb{R}^3$ an observation domain with volume $0 < \nu(K) < \infty$. A PP on K is a finite configuration of points $\{k_i \in K, i = 1, ..., N\}$ as $k_i \neq k_j$ for $i \neq j$. To form more complex objects, we can attach characteristics or marks to the points. Let $(M, \mathcal{M}, \nu_M)$ be the probability space which describes the marks. A finite random configuration of marked points (or objects) is a sample of a MPP if only the position process of objects is a PP. Based on this definition, volume or image features are viewed as a set of objects identified jointly by their positions in the image and their geometrical characteristics.

The simplest MPP in K is the Poisson MPP. Thus, the number of objects is chosen from a Poisson distribution, and the points representing the positions of the objects are uniformly distributed in K. The marks are chosen independently for each point. For a more complete presentation of MPP, the reader is referred to [11, 12]).

2.2. Proposed model

Our aim is to reconstruct a volume of 3D particles based on the light energy acquired in the projections (images). Unlike classic tomographic reconstruction methods, the objective is to obtain 3D particles that belong to a continuous 3D space (*i.e.* a position of a 3D particle belongs to $\mathbb{R}^3$). Following the elements recalled in section 2, points are center positions of 3D particles and marks provide center intensities, forms and radiuses. Thus, such configuration of 3D particles is given by $y = \{(k_1, m_1), ..., (k_N, m_N)\}$, with $k_i \in K$ and $m_i \in M$, the 3D particle positions and the 3D particle marks, respectively, $\forall\ 1 \leq i \leq N$. This process provides a naturally sparse representation of configurations of objects of interest which are inside a volume. They allow a detachment from the numerical model induced by the volume constituted of voxels, to better approximate the physical model.

A configuration of a MPP is classically viewed as a sample issued from an unnormalized probability density f which is a Gibbs distribution:

$$f(y|\theta) \propto exp(-U(y|\theta)) \tag{1}$$

with y is a finite configuration of 3D particles and θ a set of fixed parameters. The energy $U(y|\theta)$ allows the modeling of interactions between particles and is composed of the sum of two terms: 1) a data driven energy denoted $U_d(y|\theta_d)$ that reflects the adequacy between configurations of 3D particles and the observed data and 2) an internal energy denoted $U_i(y|\theta_i)$ that reflects an a priori on such configurations. This leads to the following expression:

$$U(y|\theta) = U_d(y|\theta_d) + U_i(y|\theta_i) \tag{2}$$

and $\theta = \theta_d \cup \theta_i$. Thus, for a given value of θ parameters, the most likely configuration which allows the volume reconstruction corresponds to the global minimum of the total energy:

$$\widehat{y} = \underset{y}{\operatorname{argmin}}\ U(y|\theta) \tag{3}$$

The computation of the minimum of the energy is performed by a simulated annealing which is a stochastic method of optimization [13, 14]. This technique is based on the simulation of a non-homogeneous Markov Chain (see [9, 15] for example and section 3 for implementation details).

An appropriate definition of the data energy allows to obtain consistent marked points (particles) compared to a given observation. In our case, this energy will enable the process to converge to an appropriate configuration of 3D particles given the acquired images.

2.2.1. Data driven energy

This section provides the main contribution of the paper: the proposition of a data driven energy. This has been obtained from the mean square error (MSE) between the projection of the population of 3D particles y and the acquired images:

$$MSE(y) = \frac{1}{\sum_{i=1}^{n} |I_i|} \sum_{i=1}^{n} \sum_{s \in I_i} (o_{i,s} - r_{i,s})^2 \tag{4}$$

where n is the number of projections. $\{s\}$ is the set of the sites (pixels) of the projections (images) and $o_{i,s}$ corresponds to the observed value at the site s of the projection I_i whose cardinal is $|I_i|$, $i = 1, \ldots, n$. $\{r_{i,s}\}$ is the set of projected values computed from the population y. The computation of the set of values implies a procedure of discretization of each 3D particle in n discrete 2D particles, each one associated to a projection. Thus, $r_{i,s}$ is the sum of the contributions of each 3D particle $y_j \in y$ which has a non zero intensity at site s of its projected discrete 2D particle in I_i. We will denote this property $y_j \rightarrow s$. Then, $r_{i,s} = \sum_{y_j, y_j \rightarrow s} r_{y_j \rightarrow s}$ with $r_{y_j \rightarrow s}$ is the intensity projected by y_j at site s of I_i.

Following the previous definitions, we develop $MSE(y)$ and the deletion of constant terms allows us to obtain the expression of a data driven energy in the form of a sum of two energies $U_{d,1}(y|\theta_d) + U_{d,2}(y|\theta_d)$ defined as follows:

$$U_{d,1}(y|\theta_d) = \sum_{y_j \in y} \phi_{d,1}(y_j) \tag{5}$$

where $\phi_{d,1}(y_j) = \sum_{i=1}^{n} \sum_{s \in I_i, y_j \rightarrow s} r_{y_j \rightarrow s} \left(r_{y_j \rightarrow s} - 2o_{i,s} \right)$ and

$$U_{d,2}(y|\theta_d) = \sum_{i=1}^{n} \sum_{y_j \overset{i}{\sim} y_k, j<k} \phi^i_{d,2}(y_j, y_k) \tag{6}$$

where $\phi^i_{d,2}(y_j, y_k) = \sum_{s \in I_i} 2 r_{y_j \rightarrow s} r_{y_k \rightarrow s}$. Note that $\overset{i}{\sim}$ defines a neighboring property between two 3D particles ($y_j \overset{i}{\sim} y_k$ if $y_j \rightarrow s$ and $y_k \rightarrow s$) that models their interactions based on the correlation between their projected values on a given image.

For a given particle y_j, $\phi_{d,1}(y_j)$ is high when the values in the observed images are low, thus increasing the value of U. Conversely, when the values in the observed images are high, $\phi_{d,1}(y_j)$ is negative and then favors the corresponding position of the associated 3D particle. $\phi_{d,2}(y_j, y_k)$ penalizes two particles which have same projections in an image. The data driven energy will be at a minimum for a set of correctly positioned 3D particles which have not too many similar projections, a desired configuration of 3D particles.

2.2.2. Internal energy

In the proposed model, the energy function is divided on a sum of two terms and can be written as follows:

$$U_i(y|\theta_i) = U_e(y|\theta_e) + U_s(y|\theta_s) \tag{7}$$

The first term $U_e(y|\theta_e) = -n(y)\log(\beta)$ is an energy associated with the intensity of the process in terms of number of particles $n(y)$ in a configuration. It is defined by the parameter β, which represents the mean number of points by unity of volume. The second term $U_s(y|\theta_s) = -n_a(y)\log(\gamma_a)$ allows the definition of a Strauss point process which belongs to the family of Markov point processes [7, 15]. When $0 \leq \gamma_a < 1$, this component penalizes aggregation of 3D particles. $n_a(y)$ represents the number of neighbor relationships between 3D particles in the following sense: $y_i \overset{S}{\sim} y_j$ if $||k_i - k_j||_2 \leq r_i + r_j$ where r_i and r_j are the radiuses of y_i and y_j respectively. The value of the hyper-parameter $\gamma_a \in [0, 1]$ controls the outcome of the potential function. If $\gamma_a = 1$, the process defined by U_i behaves as an homogeneous Poisson PP with intensity β. If $\gamma_a \in]0; 1[$, pairs of 3D particles with distance less than $r_i + r_j$ are penalized. If $\gamma_a = 0$, the process forbids that two points exist within distance $r_i + r_j$ of each other. The process is then said to be hard core.

The proposed model is then parameterized by $\theta = \theta_d \cup \theta_i$ with $\theta_i = \{\beta, \gamma_a\}$. θ_d is mainly defined by the model of the 3D particles (minimum and maximum values for their intensities and radiuses) and the way they are projected on images.

2.3. Simulation of Point Processes

PP and MPP are classically simulated using Reversible Jump Markov Chain Monte Carlo method (RJMCMC) exploiting a Metropolis-Hasting-Green (MHG) dynamic [8, 16, 17, 18]. This dynamic allows the simulation of a process with varying sampling spaces. In our case, these sampling spaces are associated with configurations with different numbers of particles. The basic moves of RJMCMC for MPP are the birth and death moves [7, 19, 20]: at each iteration, one object is either added to or removed from the current configuration.

Let us denote f_b the probability to select the birth move, and f_d the probability to choose a death move. In the birth move case, the position of the new particle ξ is chosen randomly following a uniform distribution on the volume K. Therefore, the proposed state is $y' = y \cup \{\xi\}$ and the following Metropolis-Hastings-Green ratio is obtained:

$$\tau_B = \frac{f_d}{f_b} \frac{f(y'|\theta)}{f(y|\theta)} \frac{\nu(K)}{n(y)+1} \tag{8}$$

In the death move case, the point to be removed is chosen with a uniform probability on the existing points in the configuration. the proposed state is $y' = y \setminus \{\xi\}$ and the following Metropolis-Hastings-Green ratio is obtained:

$$\tau_D = \frac{f_b}{f_d} \frac{f(y'|\theta)}{f(y|\theta)} \frac{n(y)}{\nu(K)} \tag{9}$$

(see Sec. 2.1 for $\nu(K)$ and Eq.(1) for $f(y|\theta)$). The different propositions are accepted with probability $\min\{1, \tau_i\}$, $i = B$ or D. In each case, the ratio $\frac{f(y'|\theta)}{f(y|\theta)} = \exp\{-\Delta U\}$, with $\Delta U = U(y'|\theta) - U(y|\theta)$, only depends on the terms associated to the added or deleted particle. For example, in the case of a birth:

$$\Delta U = \phi_{d,1}(\xi) + \sum_{i \in I_i} \sum_{y_j \overset{i}{\sim} \xi} \phi^i_{d,2}(y_j, \xi) - \log\left(\beta \gamma_a^{n_\xi}\right) \tag{10}$$

where n_ξ is the number of neighbors of ξ following the $\overset{S}{\sim}$ neighbor relationship (see Sec. 2.2.2).

The initial configuration of 3D particles can be chosen in order to speed up the convergence of the simulated annealing. This paper does not deal with the problem of initialization and the initial configuration is the one with no particle.

3. RESULTS

In this section, we present results of 3D particles volume reconstruction. The method described above was applied on simulated data. These data were created by an image generator developed during the previous project on Tomography using SLIP library [21].

The size of the simulated volume was $200 \times 200 \times 50$ voxels and it contained 50 particles. Four projections of size 200×200 pixels, each one containing 50 particles were then computed. 2D and 3D particles are characterized by marks as described in 2.2. In this simulation, we fixed the intensity center of all particles. The size was $5 \times 5 \times 5$ voxels for 3D particles and 3×3 pixels for 2D particles. The intensity shape of all particles was modeled as a multivariate isotropic Gaussian density and the particles had a spherical form. The 3D particles were projected with angle of 30° and a Pinhole camera model is used.To be closer to the real case, we added a Poisson noise to the four projections with a percentage value equal to 0.1%. These noisy projections provide the simulated observed data (see left column of Fig. 3).

The parameters of the proposed model must be chosen carefully in order to get a good reconstruction of 3D particle volume. The intensity parameter β was fixed to $25\ .10^{-6}$ while the γ_a parameter was fixed to $\gamma_a = 0.05$. f_b and f_d denote the probability to select "Birth" and "Death" moves respectively ($f_d = 1 - f_b$). The birth probability f_b was fixed to 0.3 and the death probability f_d was fixed to 0.7.

The simulated annealing algorithm is configured with an initial temperature T_0 equal to 2 and with a fixed final temperature T_f equal to 0.1. We chose a classical cooling scheme: $T_t = T_0\ q^t$ with t the current iteration and q the parameter of the cooling scheme with $q = \left(\frac{T_f}{T_0}\right)^{\frac{1}{N_{it}}}$ and N_{it} the number of iterations.

The RJMCMC dynamics was run for $N_{it} = 2.5\ .10^6$ iterations. One iteration corresponds to one proposed birth/death move, which may be accepted or not. These choices of parameters were adopted after several simulations, compromising between the quality of the reconstruction and presence of ghost particles.

Therefore, for an empirical evaluation of our method, some graphical tests have been derived. In figure 2, the sum of MSE between the simulated projections and the generated projections are plotted. This figure shows that the MSE decreases with the iterations. The minimal value of the MSE is equal to $7.4\ .10^{-4}$ and it is obtained for $t = 1.5\ .10^6$.

The right column of the figure 3 presents the four projections that have been generated from the process. Each projection contains 50 particles. Indeed, the obtained configuration contains 50 3D particles with zero false positive alert. However, some errors on the particles' position were observed.

To compare the position of the generated 3D particles with the reference, we reconstruct 10 samples (volumes) with 50 particles and compute the mean error on the 3D position. Global mean error was 0.56 voxels. In table 1, we present the mean error and the variance of the error on X, Y and Z axes. These first results have been obtained after 5 minutes on a 2.9 GHz (dual core) CPU and they are very encouraging.

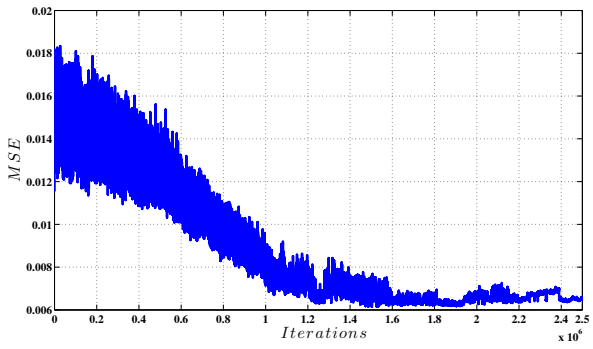

Fig. 2. Evolution of MSE during simulated anneling

	X	Y	Z
Error (voxel)	0.23	0.16	0.40
Variance (voxel)	0.18	0.23	0.09

Table 1. Mean error and variance on X, Y and Z

To compare with an existing method, we use the minLOS - MART (minimum Line Of Sight - MART) [22], an improved version of MART algorithm, to reconstruct the 3D particle volume using the simulated projections. This version, developed in Pprime institute using SLIP library [21], removes voxels and pixels which have zero energy. The MART method reconstructed the 50 particles of the simulated volume. It was observed that the 3D particles's sizes varied from one particle to another and there were some 3D particles with no gaussian form. To evaluate the quality of the reconstruction, we computed the MSE between the reconstructed volume and the original one. The MSE was equal to $2.09\ .10^{-5}$ with the proposed method against $2.20\ .10^{-5}$ with the MART method. The reconstruction of one 3D particle volume, using the simulated data, required disk space equal to 0.07 MB for our method against 15 MB for the minLOS - MART method.

4. CONCLUSION AND PERSPECTIVE

In this paper, we presented a method for 3D particle volume reconstruction using marked point process framework. Rather than pixel-oriented, our work uses object-oriented approach based on a RJMCMC method. Optimization is done with a simulated annealing method. We showed, on a simulated case, the relevance of the proposed data driven energy for the reconstruction of a volume of 3D particles. On the given example, the proposed method gives better results than the MART algorithm.

Future work will include the definition of new moves in the RJMCMC method in order to improve the positions of 3D particles and to change the radius and the center intensity of each particle. A better initialization of the population of 3D particles should be also integrated in order to speed up the convergence of the simulated annealing. The method will also be tested on real images in order to see its capacity to reconstruct a 3D velocity field. We notice that the proposed approach is in a prototype phase and the optimization of the computation time is among the first next goals of this work.

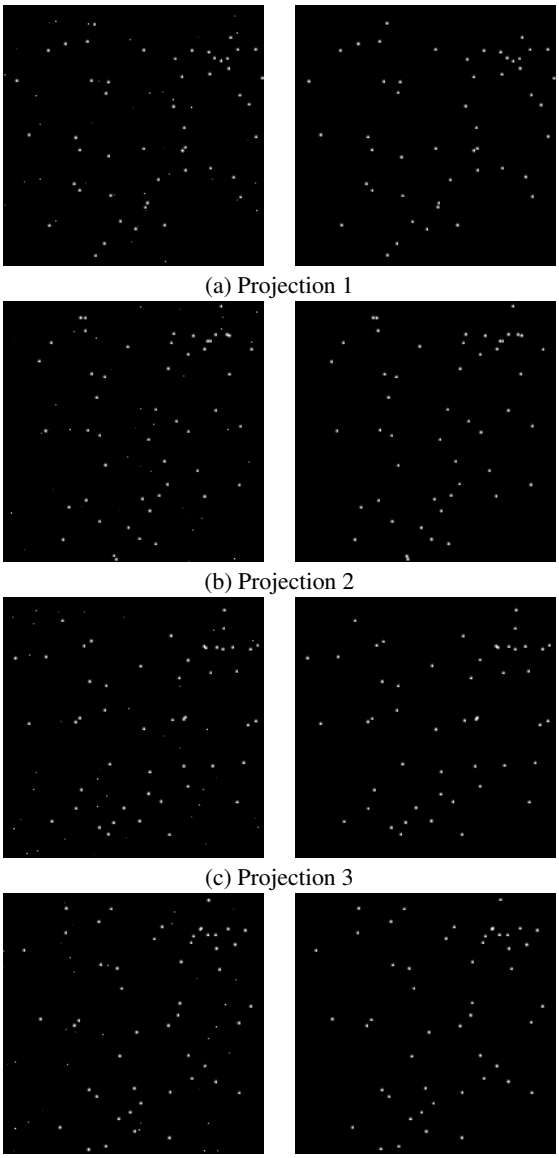

(a) Projection 1

(b) Projection 2

(c) Projection 3

(d) Projection 4

Fig. 3. Simulated images (left column) and generated images from projected 3D particles (right column)

5. REFERENCES

[1] Elsinga G. E., Scarano F., and Wieneke B., "Tomographic particle image velocimetry," *Exp Fluids*, vol. 41, pp. 933947, 2006.

[2] Gordon R., "A tutorial on art (algebraic reconstruction techniques)," *Nuclear Science, IEEE Transactions on*, vol. 21, no. 3, pp. 78–93, 1974.

[3] Herman G. T. and Arnold L., "Iterative reconstruction algorithms," *Comput. Biol. MA.*, vol. 6, no. 4, pp. 273–294, 1976.

[4] Worth N. and Nickels T., "Acceleration of tomo-piv by estimating the initial volume intensity distribution," *Experiments in Fluids*, vol. 45, pp. 847–856, 2008, 10.1007/s00348-008-0504-6.

[5] Atkinson C. H. and Soria J., "An efficient simultaneous reconstruction technique for tomographic particle image velocimetry," *Experiments in Fluids*, vol. 47, no. 4-5, pp. 553–568, 2009.

[6] Wieneke B., "Iterative reconstruction of volumetric particle distribution," *Measurement Science and Technology*, vol. 24, no. 2, pp. 024008, 2013.

[7] Van Lieshout M. N. M., *Markov point processes and their applications*, Imperial College Press/World Scientic Publishing,, 2000.

[8] Stoica R., Descombes X., and Zerubia J., "A gibbs point process for road extraction from remotely sensed images," *Int. J. Comput. Vision*, vol. 57, no. 2, pp. 121–136, May 2004.

[9] Stoica R., Martinez V., Mateu J., and Saar E., "Detection of cosmic filaments using the candy model," *Astron.Astrophys*, vol. 434, pp. 423–432, 2005.

[10] Chatelain F., Costard A., and Michel O. J J, "A bayesian marked point process for object detection. application to muse hyperspectral data," in *Acoustics, Speech and Signal Processing (ICASSP), 2011 IEEE International Conference on*, 2011, pp. 3628–3631.

[11] Stoyan D., Kendall W. S., and Mecke J., *Stochastic geometry and its applications*, John Wiley and Sons, 1995.

[12] Daley D. J. and Vere-Jones D., *An Introduction to the Theory of Point Processes: Volume I: Elementary Theory and Methods, Second Edition*, vol. 1, Springer, New York, 2nd edn. springer edition, 2003.

[13] Geman S. and Geman D., "Stochastic relaxation:gibbs distributions and the bayesian restoration of images," *IEEE Transactions on Pattern Analysis and Machine Intelligence*, vol. 9, pp. 721741, 1984.

[14] Azencott R., *Simulated annealing: Parallelization techniques*, Springer-Verlag, NY, 1992.

[15] Alata O., Burg S., and Dupas A., "Grouping/degrouping point process, a point process driven by geometrical and topological properties of a partition in regions," *Computer Vision and Image Understanding*, vol. 115, pp. 13241339, 2011.

[16] Green P. J., "Reversible jump markov chain monte carlo computation and bayesian model determination," *Biometrika*, vol. 82, no. 4, pp. 711–732, 1995.

[17] Perrin G., Descombes X., and Zerubia J., "2d and 3d vegetation resource parameters assessment using marked point processes," in *Pattern Recognition, 2006. ICPR 2006. 18th International Conference on*, 2006, vol. 1, pp. 1–4.

[18] Weina G. and Collins R.T., "Marked point processes for crowd counting," in *Computer Vision and Pattern Recognition, 2009. CVPR 2009. IEEE Conference on*, 2009, pp. 2913–2920.

[19] Preston C. J., "Spatial birth-and-death processes," *Bulletin of the International Statistical Institute*, vol. 46, pp. 371391, 1977.

[20] Baddeley A. J. and Lieshout M. N. M. Van, "Stochastic geometry models in high-level vision," *Journal of Applied Statistics*, vol. 20, no. 5-6, pp. 231–256, 1993.

[21] Tremblais B., David L., Arrivault D., Dombre J., Chatellier L., and Thomas L., "Slip : Simple library for image processing (version 1.0)," http://www.sic.sp2mi.univ-poitiers.fr/slip/, 2010.

[22] Putze T. and Maas H-G., "3d determination of very dense particle velocity fields by tomographic reconstruction from four camera views and voxel space tracking," *The International Archives of the Photogrammetry, Remote Sensing and Spatial Information Sciences*, vol. 37, no. 1, pp. 33–38, 2008.